Neuroimaging of Traumatic Brain Injury

Tuong H. Le, MD, PhD, and Alisa D. Gean, MD

Department of Radiology, Brain and Spinal Cord Injury Center, San Francisco General Hospital, San Francisco, CA

ABSTRACT

In this article, the neuroradiological evaluation of traumatic brain injury is reviewed. Different imaging strategies in the assessment of traumatic brain injury are initially discussed, and this is followed by a review of the imaging characteristics of both primary and secondary brain injuries. Computed tomography remains the modality of choice for the initial assessment of acute head injury because it is fast, widely available, and highly accurate in the detection of skull fractures and acute intracranial hemorrhage. Magnetic resonance imaging is recommended for patients with acute traumatic brain injury when the neurological findings are unexplained by computed tomography. Magnetic resonance imaging is also the modality of choice for the evaluation of subacute or chronic traumatic brain injury. Mild traumatic brain injury continues to be difficult to diagnose with current imaging technology. Advanced magnetic resonance techniques, such as diffusion-weighted imaging, magnetic resonance spectroscopy, and magnetization transfer imaging, can improve the identification of traumatic brain injury, especially in the case of mild traumatic brain injury. Further research is needed for other advanced imaging methods such as magnetic source imaging, single photon emission tomography, and positron emission tomography. ***Mt Sinai J Med 76:145–162, 2009.*** © *2009 Mount Sinai School of Medicine*

Address Correspondence to:

Alisa D. Gean, MD
Department of Radiology
Brain and Spinal Cord Injury Center
San Francisco General Hospital
San Francisco, CA
Email: alisa.gean@radiology.ucsf.edu

Key Words: brain herniation, cerebral edema, diffuse axonal injury, epidural hematoma, intracerebral hematoma, intraventricular hemorrhage, subarachnoid hemorrhage, subdural hematoma, traumatic brain injury.

Traumatic brain injury (TBI) refers to an injury to the intracranial structures following physical trauma to the head. The term *head injury* is preferred when we are addressing injuries that encompass both intracranial and extracranial structures, including the scalp and skull. Clinical classification of the severity of TBI is usually based on the Glasgow Coma Scale (GCS; mild: $12 > GCS \leq 15$; moderate: $8 > GCS \leq 12$; severe: $GCS \leq 8$).[1] In the neuroradiological evaluation of head trauma, TBI is usually classified into primary and secondary injuries (Table 1). Primary injuries are the direct result of trauma to the head. Secondary injuries arise as complications of primary lesions. This classification is important because secondary injuries are potentially preventable, whereas primary injuries, by definition, have already occurred by the time the patient first presents for medical attention. TBI can be further divided according to location (intra-axial or extra-axial) and mechanism (penetrating/open or blunt/closed). The goal of neuroimaging is to identify treatable injuries to prevent secondary damage and to provide useful prognostic information. In this article, a discussion of the different imaging options for TBI is followed by a review of the imaging characteristics of primary and secondary TBI.

METHODS

A search was performed at http://www.ncbi.nlm.nih.gov/sites/entrez (National Center for Biotechnology Information and National Library of Medicine) using '[Text Word]' search with the search terms *traumatic* AND *brain*, AND '[Title]' search with search term *imaging*, which resulted in 240 articles published in English since 1978. Among these 240 articles,

Published online in Wiley InterScience (www.interscience.wiley.com).
DOI:10.1002/msj.20102

Table 1. *Imaging Classification of Traumatic Brain Injury.*

Primary injury
Extra-axial injury
Epidural hematoma
Subdural hematoma
Subarachnoid hemorrhage
Intraventricular hemorrhage
Intra-axial injury
Axonal injury
Cortical contusion
Intracerebral hematoma
Vascular injury
Dissection
Carotid cavernous fistula
Arteriovenous dural fistula
Pseudoaneurysm
Secondary injury
Acute
Diffuse cerebral swelling/dysautoregulation
Brain herniation
Infarction
Infection
Chronic
Hydrocephalus
Encephalomalacia
Cerebrospinal fluid leak
Leptomeningeal cyst

39 were review articles. Abstracts from the 240 articles were examined. Selected articles from the 240 abstracts and key articles referenced by some of the selected articles, relevant to the objectives of our article, were reviewed. These articles include both pediatric and adult populations.

Most images published in our article were derived from the Teaching File Server (http://tfserver.ucsf.edu), which is the property of the Department of Radiology, University of California. Images on the server have been submitted over the years by the attendings, fellows, and residents in the Department of Radiology at Moffit-Long Hospital, the VA Medical Center, and San Francisco General Hospital. Patient demographics were removed in compliance with the Health Insurance Portability and Accountability Act.

IMAGING OPTIONS

Skull Films

Skull films are poor predictors of intracranial pathology and should not be performed to evaluate TBI.[2–4] In mild TBI, skull films rarely demonstrate significant findings. In severe TBI, the lack of abnormality on skull films does not exclude major intracranial injury.[5] Negative findings may even mislead medical management. Patients who are at high risk for acute intracranial injury must be imaged by computed tomography (CT).

Computed Tomography

CT is indicated for moderate and severe TBI (GCS $\leq$ 12) and for patients with mild TBI and age greater than 60 years, persistent neurological deficit, headache or vomiting, amnesia, loss of consciousness longer than 5 minutes, depressed skull fracture, penetrating injury, or bleeding diathesis or anticoagulation therapy.[6–12] CT is the modality of choice because it is fast, widely available, and highly accurate in the detection of skull fractures and intracranial hemorrhage. Life-support and monitoring equipment can be more easily accommodated in the CT scanner suite than in the magnetic resonance (MR) suite. In addition, CT is superior to magnetic resonance imaging (MRI) in revealing skull fractures and radio-opaque foreign bodies. Intravenous contrast administration should not be performed without a prior noncontrast examination because contrast can both mask and mimic underlying hemorrhage. In suspected vascular injury, CT angiography can be performed at a high (submillimeter) resolution, especially on multidetector CT. However, even with the tremendous advances in CT over the last 3 decades, the majority of mild TBI cases still show no visible abnormality on CT.[13]

Magnetic Resonance Imaging

MRI may be indicated in patients with acute TBI when the neurological findings are unexplained by the CT findings. MRI is also the preferred imaging modality for subacute and chronic TBI. MRI is comparable to CT in the detection of acute epidural hematoma (EDH) and subdural hematoma (SDH).[14,15] However, MRI is more sensitive to subtle extra-axial smear collections, nonhemorrhagic lesions, brainstem injuries, and subarachnoid hemorrhage (SAH) when fluid attenuated inversion recovery (FLAIR) is used.[16,17]

Fluid Attenuated Inversion Recovery

FLAIR imaging improves the detection of focal cortical injuries (eg, contusions), white matter shearing injuries, and SAH by suppressing the bright cerebrospinal fluid (CSF) signal typically seen on routine T2-weighted images. Sagittal and coronal FLAIR images are particularly helpful in the detection of diffuse axonal injury (DAI) involving the corpus callosum and the fornix, 2 areas that are difficult to evaluate on routine axial T2-weighted images.

DOI:10.1002/MSJ

However, an abnormally high signal in the sulci and cisterns of ventilated patients receiving a high inspired oxygen fraction (>0.60) can be observed in uninjured patients and should not be mistaken for hemorrhage.[18]

Gradient-Recalled-Echo T2*-Weighted Magnetic Resonance Imaging

Gradient-recalled-echo (GRE) T2*-weighted MRI is highly sensitive to the presence of ferritin and hemosiderin, 2 breakdown products of blood. The presence of hemosiderin and ferritin alters the local magnetic susceptibility of tissue, resulting in areas of signal loss on GRE T2*-weighted images. Because hemosiderin can persist indefinitely, its detection on GRE T2*-weighted images allows for improved evaluation of remote TBI. Unfortunately, GRE images are limited in the evaluation of cortical contusions of the inferior frontal and temporal lobes because of the inhomogeneity artifact induced by the paranasal sinuses and mastoid air cells. This limitation is even more problematic at higher magnetic field strengths unless parallel imaging is used.[19,20]

Diffusion-Weighted Imaging

Diffusion-weighted imaging (DWI) measures the random motion of water molecules in brain tissue. Because of its improved sensitivity to foci of acute shearing injury, DWI has been particularly useful for the detection of DAI.[21–24] DWI reveals more DAI lesions than fast spin-echo T2-weighted or GRE T2*-weighted images in patients imaged within 48 hours of injury. The apparent diffusion coefficient, which measures the magnitude of water diffusion averaged over a 3-dimensional space, is often reduced in acute DAI. The fractional anisotropy, which measures the preferential motion of water molecules along the white matter axons, is frequently reduced in chronic DAI. The integrity of white matter tracts can be evaluated with diffusion tensor imaging.

Magnetic Resonance Spectroscopy

Magnetic resonance spectroscopy (MRS) measures the relative amount of metabolites in brain tissue. Common neurochemicals that are measured with proton MRS include *N*-acetylaspartate (NAA), creatinine (Cr), choline, and myoinositol. In brief, NAA is a marker of neuronal health, and Cr is a marker of energy metabolism. A reduction in the NAA/Cr ratio has been found in patients with a history of TBI, and this finding has been correlated with a poorer prognosis.[25]

Magnetization Transfer Imaging

Magnetization transfer imaging exploits the longitudinal (T1) relaxation coupling between bound (hydration) protons and free water (bulk) protons. When an off-resonance saturation (radiofrequency) pulse is applied, it selectively saturates protons that are bound in macromolecules. These protons subsequently exchange longitudinal magnetization with free water protons. The magnetization transfer ratio provides a quantitative measure of the structural integrity of tissue. A reduction of the magnetization transfer ratio correlates with worse clinical outcome in a patient with a history of TBI.[25]

Magnetic Source Imaging

Magnetic source imaging (MSI) uses magnetoencephalography to localize weak magnetic signals generated by neuronal electrical activity. In 2 studies, MSI showed excessive abnormal low-frequency magnetic activity in mild TBI patients with postconcussive syndromes.[26,27] TBI research using MSI has been limited, and the practical application of MSI in the evaluation of TBI has not been very successful.

Single Photon Emission Tomography

Single photon emission tomography (SPECT) is a nuclear medicine study that measures cerebral blood flow (CBF). It can potentially provide a better long-term prognostic predictor in comparison with CT or conventional MRI.[28] Specifically, a worse prognosis has been associated with multiple CBF abnormalities, larger CBF defects, and defects that involve the basal ganglia, temporal and parietal lobes, and brainstem. However, SPECT is less sensitive in detecting smaller lesions that are visible on MRI. Therefore, SPECT imaging is complementary for MRI, but not a replacement, in the evaluation of TBI.

Positron Emission Tomography

Positron emission tomography measures regional brain metabolism with 2-fluoro-2-deoxy-d-glucose. In animal studies, acutely injured brain cells show increased glucose metabolism following severe TBI due to intracellular ionic perturbation. Following the initial hyperglycolysis state, injured brain cells show a prolonged period of regional hypometabolism lasting up to months.[29] Human studies in TBI have had limited success in demonstrating consistent results regarding regional glucose metabolism. Because of the heterogeneous nature of TBI, studies have found both hypermetabolism and hypometabolism in the same regions across different TBI patients.[30] The

DOI:10.1002/MSJ

metabolic abnormalities can also be found extending far beyond the lesions, especially with SDHs and EDHs.[31] Cortical contusion, intracerebral hematoma, and encephalomacia tend to show more regional metabolic abnormalities confined to the specific lesions.

PRIMARY EXTRA-AXIAL INJURY IMAGING FINDINGS

Epidural Hematoma

EDH develops within the potential space located between the inner table of the skull and the dura. The developing hematoma dissects the dura from the inner table of the skull, forming an ovoid mass that displaces the adjacent brain. Because the EDH is located in the potential space between the dura and inner table of the skull, it rarely crosses cranial sutures, where the periosteal layer of the dura is firmly attached at sutural margins (Figure 1). At the vertex, where the periosteum is not tightly attached to the sagittal suture, the EDH can cross the midline. The majority of EDHs are associated with a skull fracture, commonly in the temporal squamosa, where the fracture disrupts the middle meningeal artery.[12] In children, EDHs may occur from stretching or tearing of meningeal arteries without an associated fracture.

On CT, an acute EDH appears as a well-defined, hyperdense, biconvex extra-axial collection (Figures 2 and 3). Mass effect, sulcal effacement, and midline shift are frequently seen with large EDHs. An important imaging finding that predicts rapid expansion of an arterial EDH is the presence of low-density areas within the hyperdense hematoma (the so-called swirl sign), which is thought to represent active bleeding.[32,33] It is an ominous sign that needs to be followed closely.

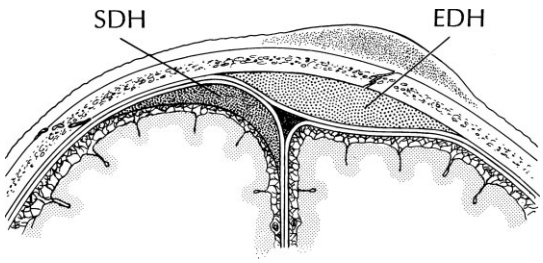

Fig 1. Coronal diagram of EDH and SDH. The EDH is located above the outer dural layer (ie, the periosteum), and the SDH is located beneath the inner (meningeal) dural layer. The EDH does not cross sutures. The SDH does not directly cross the falx or the tentorium. **Abbreviations:** EDH, epidural hematoma; SDH, subdural hematoma. Reprinted with permission from Williams & Wilkins-Lippincott.[44] Copyright 1994, Williams & Wilkins-Lippincott.

Venous EDHs are less common than arterial EDHs and tend to occur at 3 common locations: the posterior fossa from rupture of the torcula or transverse sinus, the middle cranial fossa from disruption of the sphenoparietal sinus (Figure 3), and the vertex from injury to the superior sagittal sinus.[34] Venous EDHs can be difficult to diagnose on axial CT imaging but are readily confirmed on coronal reformatted CT images or multiplanar MR images.

Subdural Hematomas

SDHs usually develop from laceration of bridging cortical veins during sudden head deceleration. They can also arise from injury to pial vessels, pacchionian granulations, or penetrating branches of superficial cerebral arteries. Because the inner dural layer and arachnoid are not firmly attached, SDHs are frequently seen layering along the entire hemispheric convexity from the anterior falx to the posterior falx (Figure 4). In elderly patients with cerebral atrophy, the increase in extra-axial space allows for increased motion between the brain parenchyma and the calvarium, resulting in an increased incidence of SDH in these patients. Another cause of SDH is rapid decompression of obstructive hydrocephalus. In this setting, the brain surface recedes from the dura more quickly than the brain parenchyma can re-expand after being compressed by the distended ventricles, and this causes disruption of the bridging cortical veins.

On CT, the acute SDH appears as a hyperdense, homogeneous, crescent-shaped extra-axial collection (Figure 5A). Most SDHs are supratentorial and are located along the convexity. They are also frequently seen along the falx and tentorium (Figure 5B). Because the SDH is often associated with parenchymal injury, the degree of mass effect seen frequently appears more severe with respect to the size of the collection.

In comparison with a normal brain, the density (attenuation) of the acute SDH is higher because of clot retraction. The density of the SDH will progressively decrease as protein degradation occurs. Rebleeding during the evolution of the SDH appears as a heterogeneous mixture of fresh blood and partially liquefied hematoma (Figures 4 and 6). A sediment level or hematocrit effect may be seen from rebleeding or in patients with clotting disorders. The chronic SDH has density similar to, but slightly higher than, that of CSF (Figure 6). The chronic SDH can be difficult to distinguish from prominent

DOI:10.1002/MSJ

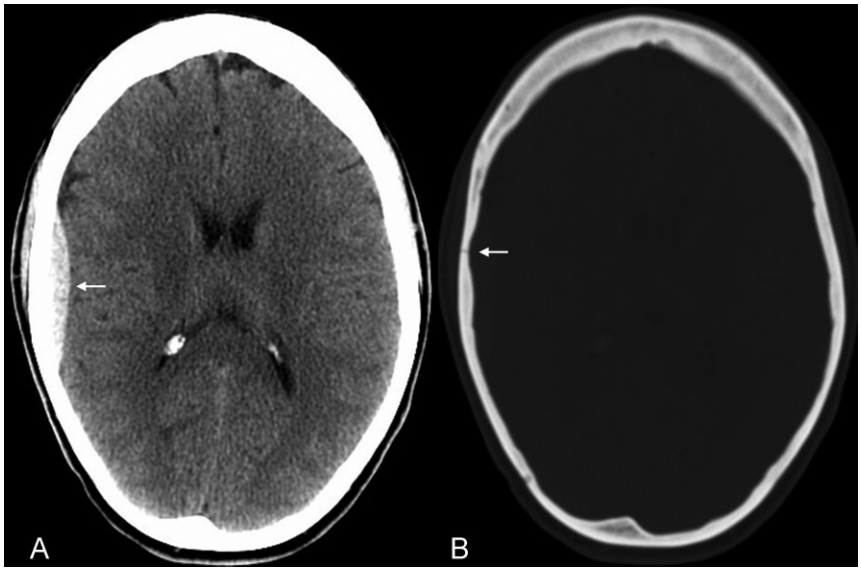

Fig 2. Acute epidural hematoma with an associated linear nondisplaced skull fracture. (A) The axial computed tomography image displayed in the brain window shows a small right temporal epidural hematoma (arrow). (B) The computed tomography scan displayed in the bone window shows a subjacent linear nondisplaced fracture of the temporal squamosa (arrow).

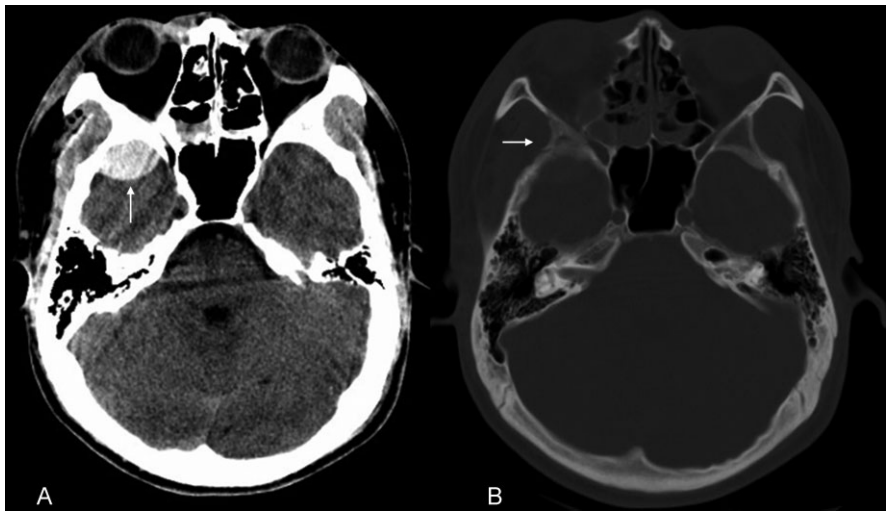

Fig 3. Venous epidural hematoma. (A) The axial computed tomography image shows a biconvex, homogeneous, high-attenuation extra-axial collection within the right middle cranial fossa (arrow). (B) The computed tomography image displayed in the bone window reveals a fracture of the right greater sphenoid wing (arrow). The location suggests that the hematoma is due to disruption of the sphenoparietal sinus.

subarachnoid space in patients with cerebral atrophy. In these patients, contrast-enhanced CT, in addition to noncontrast CT, can improve detection of the chronic SDH by demonstrating an enhancing capsule or displaced cortical veins.

In the subacute setting, usually between 1 and 3 weeks, depending on the patient's hematocrit level, clotting capability, and presence or absence of rebleeding, an isodense phase occurs. During this transition from the acute SDH to the chronic SDH, a small, thin convexity isodense SDH can be difficult to appreciate (Figure 7). Recognition of indirect imaging findings, such as sulcal effacement, gray matter displacement with white matter buckling, and midline shift, can improve detection of such isodense SDH.

DOI:10.1002/MSJ

Fig 4. Subdural hematoma with the hematocrit level. The axial computed tomography image shows a large left, holohemispheric extra-axial fluid collection. The collection is a mixture of a dense sediment level (black asterisk) and a partially liquefied hematoma (white asterisk). The attenuation gradient is secondary to the presence of hemorrhage of different ages or to a coagulopathy. There is effacement of the frontoparietal sulci, white matter buckling, and mild left-to-right midline shift resulting from the subdural hematoma mass effect.

On MRI, the acute SDH is isointense to the brain on T1-weighted images and hypointense on T2-weighted images. During the subacute phase, when the SDH may be isodense on noncontrast CT images, the SDH is a high signal intensity on T1-weighted images because of the presence of methemoglobin. The chronic liquefied SDH appears hypointense on T1-weighted images and hyperintense on T2-weighted images with respect to a normal brain (Figure 8). The signal intensity of the chronic SDH is usually slightly higher than the CSF signal intensity on T1-weighted, FLAIR, and proton-density T2-weighted images. Because of its multiplanar capability and its lack of beam-hardening artifact, which limits CT, MRI is useful in identifying small convexity and vertex hematomas that might not be readily detected on axial CT.

Traumatic Subarachnoid Hemorrhage

Traumatic SAH can develop from disruption of small pial vessels, extension into the subarachnoid space by a contusion or hematoma, or transependymal diffusion of intraventricular hemorrhage (IVH). Common sites for SAH include the sylvian and interpeduncular cisterns. The greatest accumulation of SAH tends to occur contralateral to the site of impact, that is, contrecoup.

On CT, acute SAH appears as linear or serpentine areas of high density that conform to the morphology of the cerebral sulci and cisterns (Figure 6). SAH along the convexity or tentorium can be difficult to differentiate from an SDH. A useful clue is the extension of the SAH into adjacent sulci. Occasionally, effacement of sulci due to the presence of intrasulcal SAH is the only imaging clue to the presence of SAH.

Acute SAH is more difficult to detect on T1-weighted and T2-weighted MR images than on CT because it can be isointense to brain parenchyma. However, FLAIR has been shown to be more sensitive than CT in detecting acute SAH in an animal model, especially when a high volume (1–2 mL) is present.[17] Subacute SAH, when the blood is isointense to CSF on CT, is better appreciated on MRI because of its high signal intensity. Chronic SAH is also much better seen on MRI than on CT. Ferritin and hemosiderin in the subarachnoid space appear as areas of decreased signal intensity on T1-weighted and T2-weighted images (superficial hemosiderosis). As mentioned previously, old blood products are best detected on GRE T2*-weighted images (Figure 9).

Traumatic Intraventricular Hemmorhage

Traumatic IVH can result from rotationally induced tearing of subependymal veins along the surface of the ventricles, by direct extension of a parenchymal hematoma into the ventricular system, or from retrograde flow of SAH into the ventricular system via the fourth ventricular outflow foramina. Besides hydrocephalus, patients with IVH are at risk for developing ependymitis from the irritant effects of the blood.

On CT, IVH usually appears as a CSF-hyperdense fluid level, layering dependently within the ventricular system (Figure 10). Sometimes, a tiny collection of increased density layering in 1 occipital horn may be the only clue to IVH. Occasionally, IVH may appear tumefactive as a cast within the ventricle.

PRIMARY INTRA-AXIAL INJURY

Diffuse Axonal Injury

Axonal injury refers to white matter damage arising from shearing deformation of brain tissue following rotational acceleration and deceleration injury. DAI indicates extensive injury to the white matter and occurs in about half of all severe head trauma cases.[35]

DOI:10.1002/MSJ

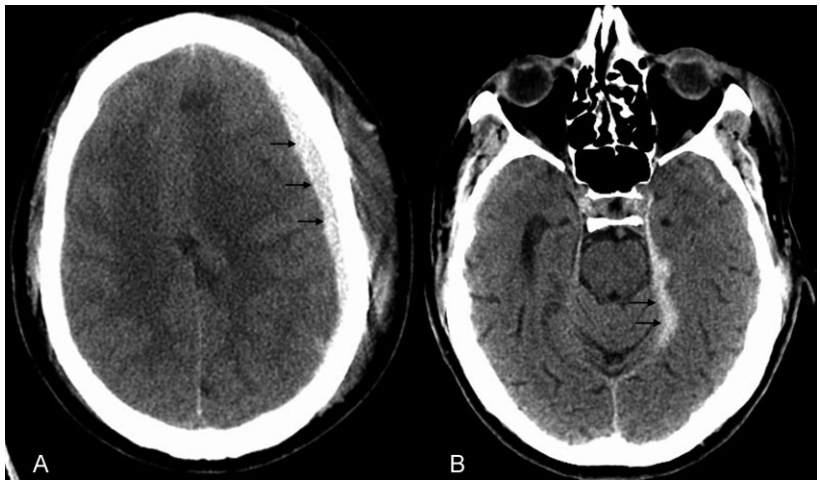

Fig 5. Acute subdural hematoma. (A) The axial computed tomography image demonstrates a left frontoparietal, hyperdense, homogeneous, crescent-shaped extra-axial collection (arrows). An overlying left frontoparietal, subgaleal hematoma is also noted. (B) The axial computed tomography image shows asymmetric hyperdensity along the left tentorium (arrows).

DAI is of special interest because it is considered to be responsible for the majority of TBI cognitive deficits, and yet it is underdiagnosed by conventional imaging techniques.[36–38]

The location of DAI has been correlated with the severity of the trauma. Specifically, mild DAI (grade I) involves only the peripheral gray-white junctions of the lobar white matter, commonly the parasagittal regions of the frontal lobes and periventricular regions of the temporal lobes. Patients with more moderate DAI (grade II) have abnormalities involving the corpus callosum, particularly the posterior body and splenium, in addition to the lobar white matter. In severe DAI (grade III), the dorsolateral midbrain, in addition to the lobar white matter and corpus callosum, is affected.

On CT, DAI lesions appear as small, petechial hemorrhages and can been seen at the gray-white junction of the cerebral hemispheres (Figure 11), corpus callosum, and dorsolateral midbrain, depending on the severity of the trauma. Because of its higher sensitivity to blood products, GRE T2*-weighted MRI identifies more hemorrhagic DAI lesions than CT.[22] However, only a minority of DAI lesions are associated with hemorrhage.[39] FLAIR MRI can uncover additional nonhemorrhagic foci of DAI but still underestimate the true extent of traumatic white matter damage.[37,40,41] Nonhemorrhagic acute DAI lesions appear as multiple small foci of increased signal on T2-weighted images and as decreased signal on T1-weighted images. In subacute DAI, intracellular methemoglobin from petechial hemorrhage appears as central hypointensity on T2-weighted images and as hyperintensity on T1-weighted images. The conspicuity of DAI on MRI eventually diminishes as the damaged axons degenerate and the edema resolves. Chronic DAI imaging findings include nonspecific atrophy, gliosis, and hemosiderin staining, which can persist indefinitely on gradient-echo T2*-weighted images (Figure 11).

Because of its superiority to CT in detecting axonal injuries, MRI helps clinicians explain neurological deficits after trauma and predict long-term outcome. Yet, even with MRI, the incidence of DAI is still underestimated. Newer imaging methods, such as DWI and diffusion tensor imaging with 3-dimensional tractography, have shown potential in improving the detection of white matter injury in both acute and chronic DAI.[22,23,42] MRS and magnetization transfer imaging can also provide additional prognostic value in DAI.[25]

Cortical Contusion

Cortical contusion is a focal brain lesion primarily involving superficial gray matter, with relative sparing of the underlying white matter. Regions of the brain that are in close contact with the rough surface on the inner skull table are commonly affected. Therefore, the temporal lobes above the petrous bone or posterior to the greater sphenoid wing are frequently affected. The frontal lobes above the cribriform plate, planum sphenoidale, and lesser sphenoid wing are also commonly involved. Contusions along the parasagittal convexity are less common. Contusions can also occur at the margins of depressed skull fractures. The cerebellum is involved

DOI:10.1002/MSJ

Fig 6. Chronic subdural hematoma with rebleeding, acute subarachnoid hemorrhage, and subgaleal hematoma. The axial computed tomography image shows a small low-density, left frontal extra-axial collection consistent with a chronic subdural hematoma (black arrows). There is also a tiny right frontal subdural collection with mixed high and low densities, which is consistent with rebleeding within a chronic subdural hematoma (horizontal white arrows). Linear high attenuation conforming to the sulci of the posterior right frontal lobe is consistent with acute subarachnoid hemorrhage (vertical white arrows). A large subgaleal scalp hematoma is noted at the coup site (asterisk).

Fig 7. Isodense subacute subdural hematoma. During the transition from an acute subdural hematoma to a chronic subdural hematoma, an isodense phase occurs. At this stage, the subdural hematoma (asterisk) can be difficult to differentiate from the adjacent parenchyma. Note the effacement of the subjacent sulci (arrows), which serves as an important clue in detecting subtle subdural hematomas.

less than 10% of the time.[43] Contusions are associated with a better prognosis than DAI unless they are accompanied by brainstem injury or significant mass effect.

On CT, hemorrhagic contusions appear as areas of high density within superficial gray matter (Figure 12). They may be surrounded by larger areas of low density from the associated vasogenic edema. As the contusion evolves, the characteristic salt and pepper pattern of mixed areas of hypodensity and hyperdensity becomes more apparent. Nonhemorrhagic contusions appear as low-attenuation areas and can be difficult to detect initially until the development of associated edema.

On MRI, contusions appear as ill-defined areas of variable signal intensity on both T1-weighted and T2-weighted images, depending on the age of the lesions (Figure 12). Again, because contusions are limited to the surface of the brain, they often have a gyral morphology. Hemosiderin from an old contusion can persist indefinitely and serves as an important marker of prior TBI.

Intracerebral Hematoma

The intracerebral hematoma is shear-induced hemorrhage due to the rupture of small intraparenchymal blood vessels. Because the bleeding occurs in areas of relatively normal brain, intracerebral hematomas usually have less surrounding edema than cortical contusions. Most traumatic intracerebral hematomas are located in the frontotemporal white matter. Involvement of the basal ganglia has been described; however, hemorrhage in basal ganglia should alert the clinician that an underlying hypertensive bleed may be the culprit (Figure 13). Intracerebral hematomas are often associated with skull fractures and other primary intracranial injuries, including contusions and DAI, especially in patients who are unconscious at the time of injury. Intracerebral hematoma is the most common cause of clinical deterioration in patients who have experienced a lucid interval after the initial injury. Delayed hemorrhage is a common cause of clinical deterioration during the first several days after head trauma.

DOI:10.1002/MSJ

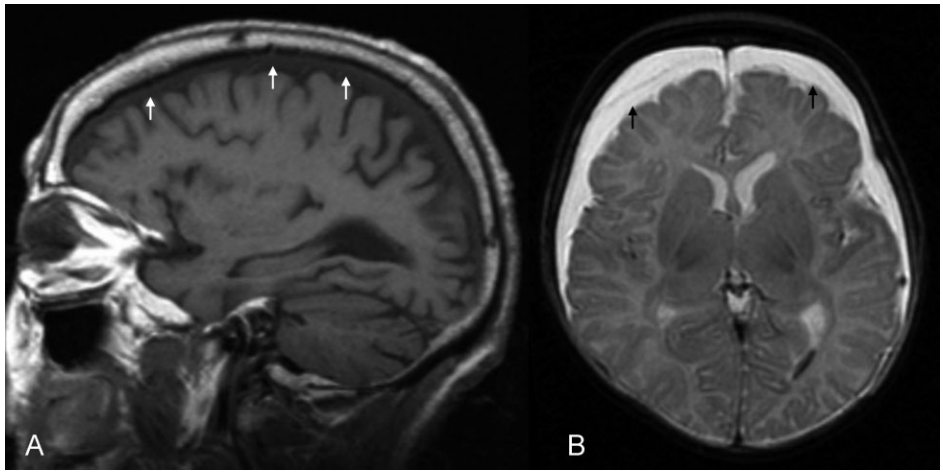

Fig 8. Appearance of the chronic subdural hematoma on magnetic resonance imaging. The chronic subdural hematoma is always slightly higher in signal intensity than cerebrospinal fluid on T1-weighted and T2-weighted images. It is (A) hypointense to gray and white matter on T1-weighted images (arrows) and (B) hyperintense to brain parenchyma on T2-weighted images. Unlike prominent subarachnoid spaces that are characteristic of cerebral atrophy, the chronic subdural hematoma causes effacement of the sulci. In addition, when rebleeding has occurred, septations may be identified within the collection (arrows).

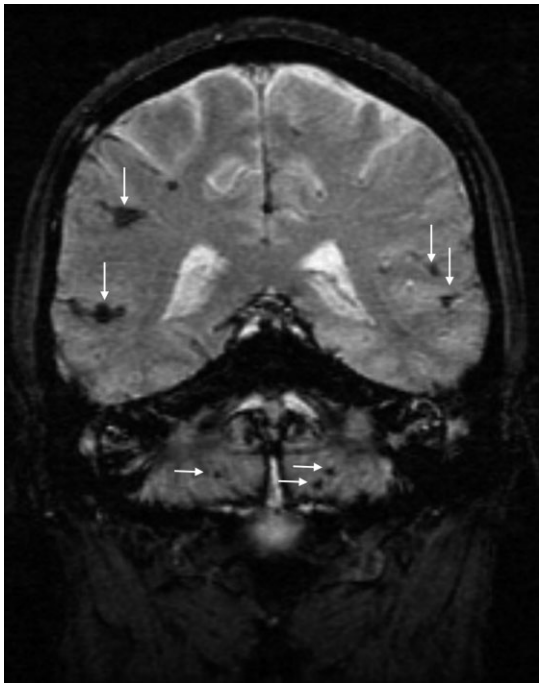

Fig 9. Chronic subarachnoid hemorrhage on magnetic resonance imaging. The coronal gradient-recalled-echo T2*-weighted image shows a low signal (vertical arrows) within the subarachnoid space of the temporal lobes and right frontal lobe due to hemosiderin deposits (superficial hemosiderosis). Foci of ferritin and hemosiderin staining within the cerebellum are also noted (white arrows), with particular involvement of the vermi.

Fig 10. Acute intraventricular hemorrhage. The axial computed tomography image shows hyperdense fluid layering within the occipital horn of the left lateral ventricle (asterisk).

DOI:10.1002/MSJ

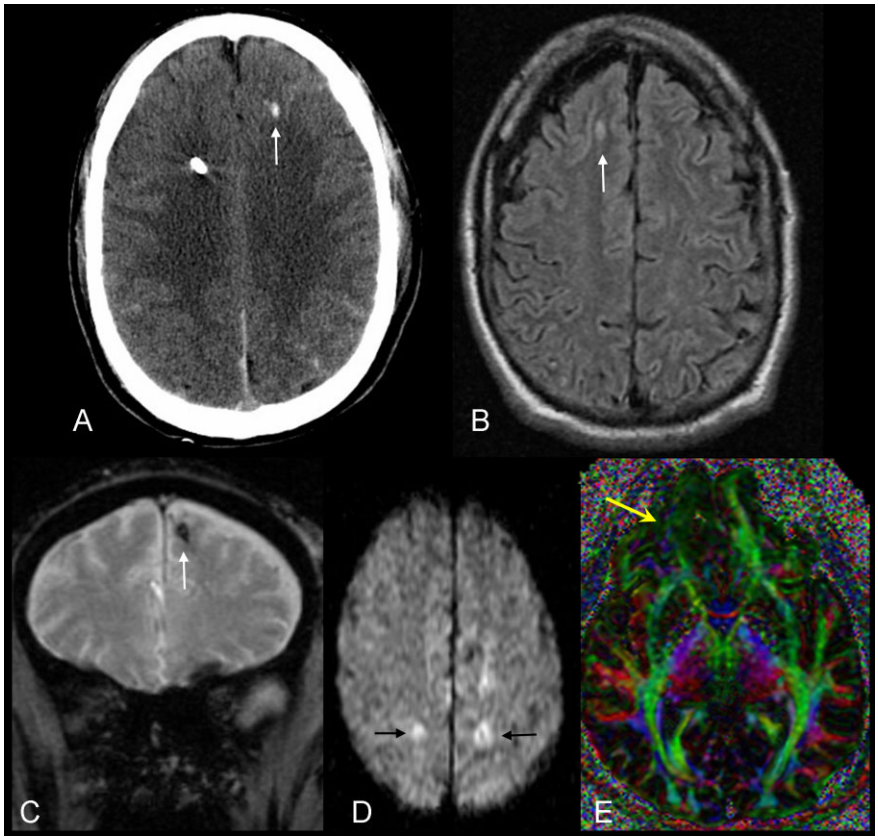

Fig 11. Diffuse axonal injury on computed tomography and magnetic resonance imaging. (A) The axial computed tomography image reveals a small hyperdense focus (arrow) at the gray-white junction of the left frontal lobe consistent with hemorrhagic diffuse axonal injury. Bilateral high attenuation with the sulci of the frontal and parietal lobes represents acute subarachnoid hemorrhage. The intensely dense focus with streak artifact within the right frontal lobe is from a ventricular drainage catheter. (B) The axial fluid attenuated inversion recovery image shows an additional lesion (arrow) within the peripheral gray-white junction of the right frontal lobe. (C) The coronal gradient-recalled-echo T2*-weighted image demonstrates a low signal focus (arrow) at the gray-white junction of the left superior frontal gyrus consistent with deoxyhemoglobin from hemorrhagic diffuse axonal injury. (D) The diffusion-weighted image shows reduced diffusion within the parietal lobe subcortical white matter bilaterally (arrows). (E) In a different patient with a history of moderate traumatic brain injury and diffuse axonal injury, the color fractional anisotropy map shows a reduction in fractional anisotropy in the white matter tract of the right inferior frontal lobe (arrow). [Color figure can be viewed in the online issue, which is available at www.interscience.wiley.com.].

VASCULAR INJURY

Vascular injuries cause both intra-axial and extra-axial injuries, including the source of hematomas and SAH described previously. Traumatic vascular injuries include arterial dissection, pseudoaneurysm, and arteriovenous fistula. Vascular injuries are usually related to skull base fractures. The internal carotid artery is the most commonly affected vessel. The injury usually occurs at sites of fixation, where the internal carotid artery enters the carotid canal at the base of the petrous bone and at its exit from the cavernous sinus beneath the anterior clinoid process.

MR findings of traumatic vascular injury include (1) the presence of an intramural hematoma, which is best seen on T1-weighted images with fat suppression (Figure 14), (2) intimal flap with dissection, and (3) the absence of a normal vascular flow void secondary to slow flow or occlusion. An associated parenchymal infarction supplied by the injured vessel may also be seen.

Conventional angiograms are the gold standard for confirmation and delineation of the vascular

DOI:10.1002/MSJ

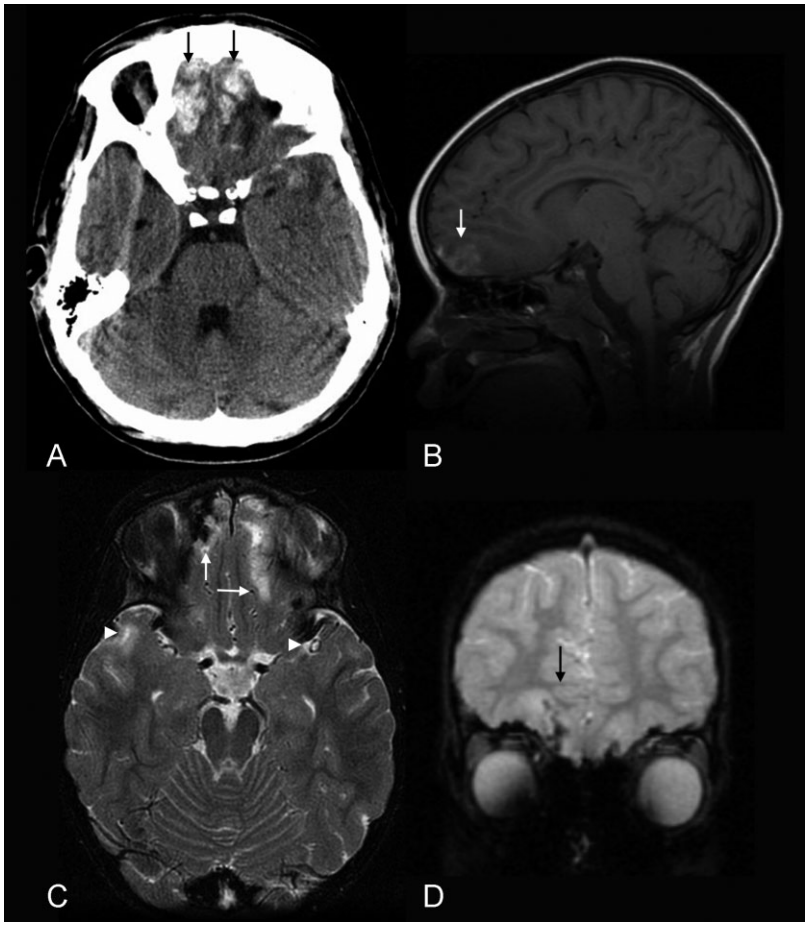

Fig 12. Computed tomography and magnetic resonance imaging of a cortical contusion. (A) The axial computed tomography image demonstrates high attenuation within the gyral crests of the bilateral orbitofrontal lobes (arrows). Partial volume artifact and streak artifact in this area are particularly problematic on computed tomography. (B) The sagittal T1-weighted image demonstrates abnormal increased signal intensity involving the right orbitofrontal lobe (arrow). (C) The axial T2-weighted image demonstrates bilateral orbitofrontal (arrows) and temporal (arrowheads) high signal. (D) The coronal gradient-recalled-echo T2*-weighted image shows decreased signal within the right orbitofrontal lobe that is consistent with blood products (arrow).

dissection and may also show spasm or pseudoaneurysm formation. However, MR angiography and multidetector CT angiography serve as important screening tools in the evaluation of patients with suspected vascular injury.

Traumatic Carotid Cavernous Fistula

The traumatic carotid cavernous fistula is a direct communication between the cavernous portion of the internal carotid artery and the surrounding venous plexus. It typically results from a full-thickness arterial injury, and it may be seen with both blunt and penetrating TBI. The fistula leads to venous engorgement of the cavernous sinus (Figure 15) and, sometimes, the ipsilateral superior ophthalmic vein and inferior petrosal sinus. Other imaging findings include retrobulbar fat stranding, proptosis, preseptal soft tissue swelling, extraocular muscle enlargement, and asymmetry of the cavernous sinus. Findings may be bilateral because venous channels connect the cavernous sinuses. In severe cases that cause intracranial venous hypertension, brain edema and hemorrhage may be seen. Skull base fractures, especially those involving the sphenoid bone, should alert the clinicians to search for associated cavernous carotid injury. Patients can present with findings weeks or even months after the initial trauma. Therefore, a carotid

DOI:10.1002/MSJ

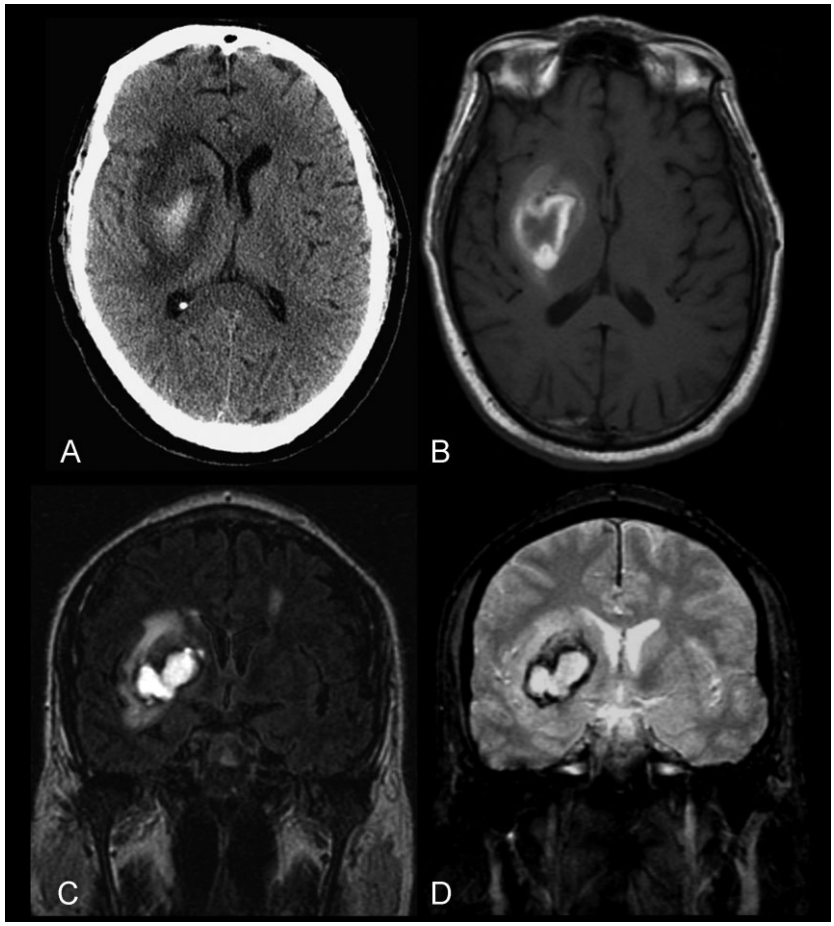

Fig 13. Intracerebral hematoma. (A) The axial computed tomography image shows a hyperdense lesion within the right putamen. The surrounding low attenuation is due to vasogenic edema. (B) On the T1-weighted image, the periphery of the hematoma is hyperintense because of the presence of methemoglobin. (C) The hematoma is also hyperintense on the fluid attenuated inversion recovery image. (D) The gradient-echo T2*-weighted image shows a surrounding hemosiderin rim, which is dark because of local magnetic susceptibility inhomogeneity. Reprinted with permission from *Seminars in Roentgenology*.[45] Copyright 2006, Elsevier.

cavernous fistula can be overlooked if a detailed clinical history and ophthalmic examination are not performed.

Arteriovenous Dural Fistula

Another traumatic vascular injury is the arteriovenous dural fistula. It is often caused by laceration of the middle meningeal artery with resultant meningeal artery to meningeal vein fistulous communication (Figure 16). Because the fistula generally drains via the meningeal veins, the injured middle meningeal artery rarely leads to the formation of an EDH. Patients are often asymptomatic or present with nonspecific complaints such as tinnitus.

ACUTE SECONDARY INJURY

Diffuse Cerebral Swelling

Diffuse cerebral swelling develops from an increase in cerebral blood volume (hyperemia) or an increase in tissue fluid (vasogenic edema and cytotoxic edema). Effacement of the cerebral sulci and cisterns and compression of the ventricles are typical findings on imaging. Hyperemia and vasogenic edema are thought to be the result of cerebral dysautoregulation, and cytotoxic edema is believed to occur secondary to tissue hypoxia. In cytotoxic edema, the gray-white differentiation is lost; this is in contrast to hyperemia, in which the gray-white differentiation is preserved. Even with cytotoxic edema, the cerebellum and brainstem are usually spared and may appear

DOI:10.1002/MSJ

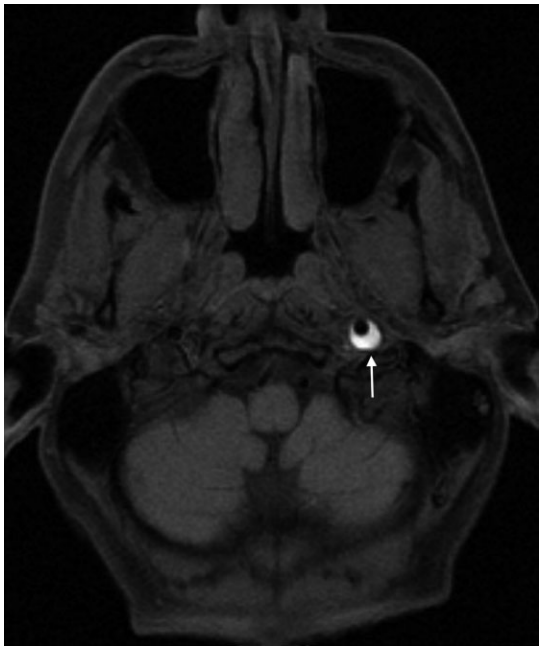

Fig 14. Carotid dissection. The T1-weighted magnetic resonance image, performed with fat suppression, shows a hyperintense crescent (arrow) beneath the adventitia of the left internal carotid artery. The high signal represents a subacute intramural hematoma. In this case, the caliber (flow void) of the vessel lumen is preserved.

Fig 15. Acquired carotid cavernous fistula. Computed tomography angiography demonstrates asymmetric enhancement of the left cavernous sinus secondary to abnormally dilated venous channels (arrow); compare this with the normal appearance of the right cavernous sinus.

hyperintense with respect to the affected cerebral hemispheres (Figure 17).

Traumatic Brain Herniation

Traumatic brain herniation occurs secondary to the mass effect produced by both primary and secondary injuries. In subfalcine herniation, the most common form of herniation, the cingulate gyrus is displaced across the midline under the falx cerebri (Figure 18). Compression of the ipsilateral ventricle due to the mass effect and enlargement of the contralateral ventricle due to obstruction of the foramen of Monro can be seen on imaging. In uncal herniation, the medial temporal lobe is displaced over the free margin of the tentorium. Effacement of the ambient and lateral suprasellar cisterns is an important clue to the presence of uncal herniation. In transtentorial herniation, the brain herniates either upward or downward because of lesions within the posterior fossa or the supratentorium. Upward herniation occurs when portions of the cerebellum and vermis displace through the tentorial incisura. With posterior fossa downward herniation, the cerebellar tonsils displace through the foramen magnum. Downward herniation of the cerebrum manifests as effacement of the suprasellar and perimesencephalic cisterns. Inferior displacement of the calcified pineal gland is another clue to the presence of downward herniation. With brain herniation, the underlying culprit must be corrected in a timely manner to prevent additional secondary injuries.

Ischemia and Infarction

Ischemia and infarction can occur because of diffuse increased intracranial pressure or a focal compressive mass effect on cerebral vasculature by herniation or hematoma. In subfalcine herniation, the anterior cerebral arteries are displaced to the contralateral side, trapping the callosomarginal branches of the anterior cerebral arteries and leading to anterior cerebral artery infarction. In severe uncal herniation, displacement of the brainstem can compress the contralateral cerebral peduncle and the posterior cerebral artery against the tentorium (Kernohan's notch), leading to peduncular infarction and/or posterior cerebral artery infarction. The third cranial nerve may also be compressed; these patients typically present with a blown pupil and ipsilateral hemiparesis. Tonsillar herniation can cause ischemia in the territory of the posterior inferior cerebellar artery distribution.

DOI:10.1002/MSJ

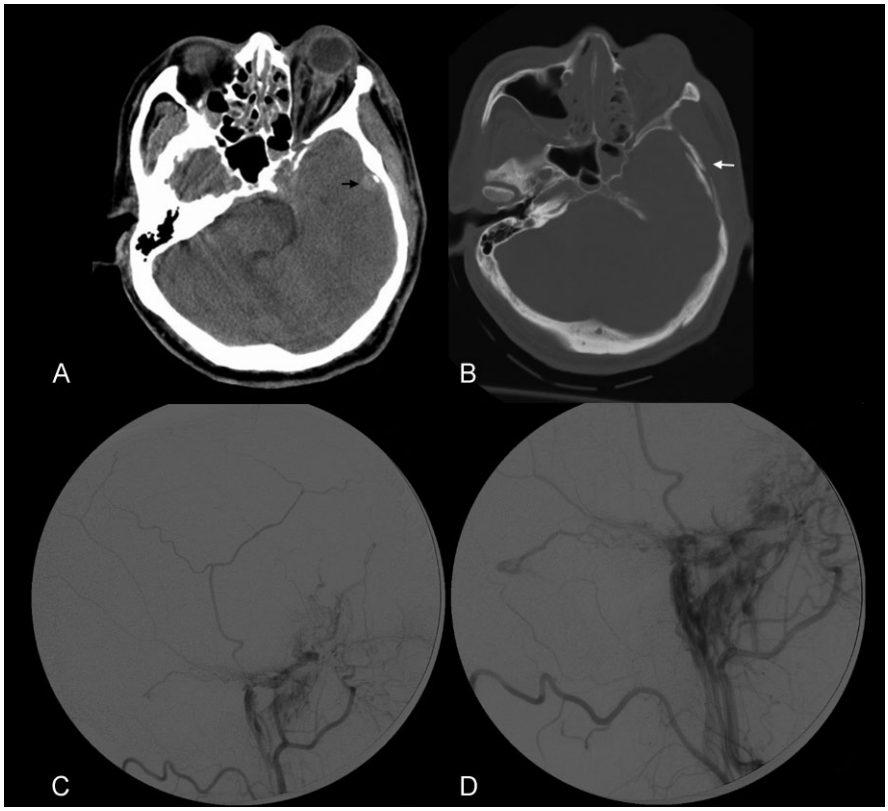

Fig 16. Dural arteriovenous fistula. (A) The axial computed tomography image displayed in the soft tissue window shows a small, round, dense, left temporal extra-axial focus (arrow). Left orbital proptosis and retrobulbar soft tissue stranding can also be seen. (B) The corresponding bone window image shows an associated temporal bone fracture (arrow). (C,D) Images from an external carotid artery cerebral angiogram in the lateral projection show blush of contrast due to filling of the middle meningeal vein via the middle meningeal artery.

CHRONIC SECONDARY INJURY

Traumatic Hydrocephalus

Traumatic hydrocephalus occurs secondary to impaired CSF reabsorption at the level of the arachnoid villi (communicating hydrocephalus) or secondary to obstruction of the cerebral aqueduct and fourth ventricular outflow (noncommunicating hydrocephalus). Hydrocephalus is not an uncommon complication seen in patients with prior SAH or IVH. A mass effect from brain herniation or a hematoma can also cause noncommunicating hydrocephalus via compression of the aqueduct and ventricular outflow foramina. On imaging, the ventricles are dilated, with associated effacement of the sulci in severe cases (Figure 19).

Encephalomalacia

Encephalomalacia is a common but nonspecific sequela of prior parenchyma injury. It is often clinically asymptomatic, but it can also be a potential seizure focus. The CT imaging appearance of encephalomalacia consists of a relatively well-defined area of low attenuation with volume loss. Encephalomalacia follows CSF signal intensity on both CT and MR, except for the areas of gliosis, which appear as low intensity on T1-weighted images and as high intensity on T2-weighted images. Encephalomalacia within the orbitofrontal (especially the gyrus rectus) and anteroinferior temporal lobes is characteristic of remote traumatic injury.

Cerebrospinal Fluid Leak

A CSF leak results from a dural tear secondary to a skull base fracture. CSF otorrhea occurs when communication between the subarachnoid space and middle ear develops in association with a ruptured tympanic membrane. CSF rhinorrhea arises when there is communication between the subarachnoid space and the paranasal sinuses. In patients with recurrent meningeal infections and a prior history

DOI:10.1002/MSJ

Fig 17. Diffuse cerebral edema. The axial computed tomography image of an infant with a history of strangulation shows a diffuse decrease in attenuation of the cerebral hemispheres with loss of gray-white differentiation. Sparing of the bilateral uncus, right frontal-temporal junction, brainstem, and cerebellum causes these structures to appear dense with respect to the rest of the brain. An acute subdural hematoma along the left tentorium is also noted.

of trauma, a CSF leak should be suspected. CSF leaks are often difficult to localize. Radionuclide cisternography is highly sensitive for the detection of CSF leaks. However, CT scanning with intrathecal contrast is required for detailed anatomic localization of the defect (Figure 20).

Leptomeningeal Cyst

The leptomeningeal cyst, a pediatric lytic calvarial lesion commonly called a growing fracture, is briefly mentioned here because it is also caused by a tear in the dura. The dural defect allows expansion of the arachnoid at the site of the bony defect, presumably as a result of CSF pulsation. Such expansion leads to progressive, slow widening of the skull defect or suture. The leptomeningeal cyst appears as a lytic skull defect on CT or plain skull films.

CONCLUSION

In this article, imaging options for TBI (Table 2) and classification of TBI have been presented. In the management of acute TBI, the goal of imaging is to identify treatable injuries to prevent secondary damages. Despite the advances in MR technology over the last 2 decades, CT continues to be the modality of choice in the evaluation of acute injury because it is fast, widely available, and highly sensitive to acute blood and can more easily accommodate life-support and monitoring equipment. MRI is indicated for patients with acute TBI when the neurological findings are unexplained by CT. MRI is also the modality of choice for subacute or chronic injury. Mild TBI continues to be underdiagnosed by imaging. Advances in MR methods, such as DWI, MRS, and magnetization transfer imaging, can further improve the neuroradiological evaluation of TBI and enhance our understanding of the pathophysiological manifestations of brain trauma. SPECT and positron emission tomography imaging can provide additional

Table 2. *Imaging Options for Traumatic Brain Injury.*

Skull film
Not recommended
Computed tomography
Recommended in the acute setting
Computed tomography cisternography for suspected cerebrospinal fluid leak
Computed tomography angiogram for vascular injury
Preferred examination for skull fractures
Magnetic resonance imaging
Recommended in the acute setting when neurological findings are unexplained by computed tomography
Recommended for subacute and chronic traumatic brain injury
Recommended for nonaccidental trauma
T1-weighted with fat suppression for suspected vascular dissection
Magnetic resonance angiogram for suspected vascular injury
Diffusion-weighted imaging for posttraumatic infarction and axonal injury
Magnetic resonance spectroscopy and magnetization transfer imaging
May be helpful in diffuse axonal injury in predicting long-term prognosis
Single photon emission tomography, positron emission tomography, and magnetic source imaging
Usefulness still limited

DOI:10.1002/MSJ

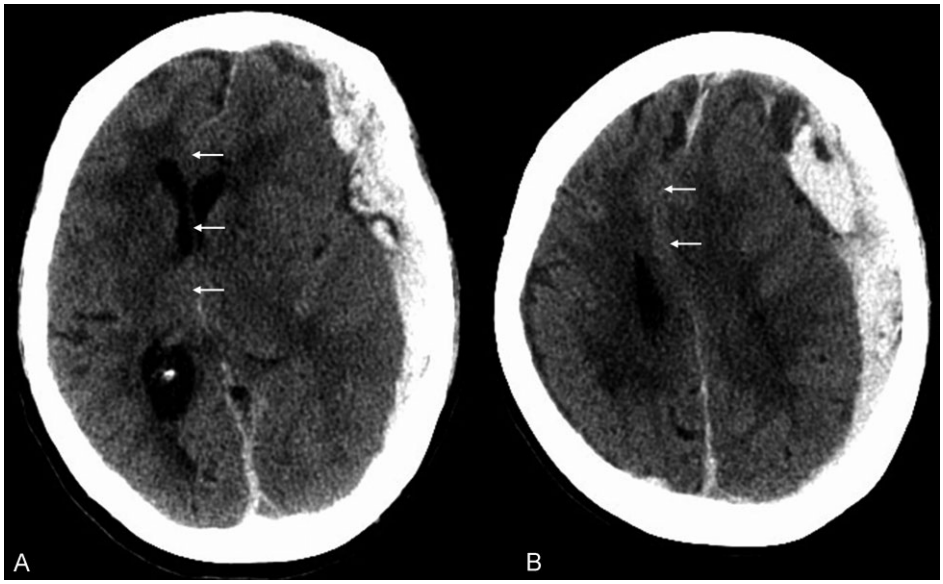

Fig 18. Subfalcine herniation due to a subdural hematoma. The axial computed tomography images show an acute, left, heterogeneous, holohemispheric subdural hematoma with associated sulcal effacement, midline shift, and left-to-right subfalcine herniation (arrows).

prognostic value, although additional research in these areas is still needed.

ACKNOWLEDGMENT

We thank the residents, fellows, and attendings from the Neuroradiology Section of the Department of Radiology, University of California San Francisco, for their continuing effort in submitting interesting cases to the teaching file server (http://tfserver.ucsf.edu). Some of the cases presented in this article were the products of their effort.

DISCLOSURES

Potential conflict of interest: Nothing to report.

REFERENCES

1. Teasdale G, Jennett B. Assessment of coma and impaired consciousness. A practical scale. *Lancet* 1974; 2: 81–84.
2. Bell RS, Loop JW. The utility and futility of radiographic skull examination for trauma. *N Engl J Med* 1971; 284: 236–239.
3. Hackney DB. Skull radiography in the evaluation of acute head trauma: a survey of current practice. *Radiology* 1991; 181: 711–714.
4. Masters SJ. Evaluation of head trauma: efficacy of skull films. *AJR Am J Roentgenol* 1980; 135: 539–547.
5. Adams J. Pathology of nonmissile head injury. *Neuroimaging Clin N Am* 1991; 1: 397–410.
6. Haydel MJ, Preston CA, Mills TJ, et al. Indications for computed tomography in patients with minor head injury. *N Engl J Med* 2000; 343: 100–105.
7. Jagoda AS, Cantrill SV, Wears RL, et al. Clinical policy: neuroimaging and decisionmaking in adult mild traumatic brain injury in the acute setting. *Ann Emerg Med* 2002; 40: 231–249.
8. Lorberboym M, Lampl Y, Gerzon I, Sadeh M. Brain SPECT evaluation of amnestic ED patients after mild head trauma. *Am J Emerg Med* 2002; 20: 310–313.
9. Stiell IG, Lesiuk H, Wells GA, et al. Canadian CT head rule study for patients with minor head injury: methodology for phase II (validation and economic analysis). *Ann Emerg Med* 2001; 38: 317–322.
10. Stiell IG, Lesiuk H, Wells GA, et al. The Canadian CT Head Rule Study for patients with minor head injury: rationale, objectives, and methodology for phase I (derivation). *Ann Emerg Med* 2001; 38: 160–169.
11. Stiell IG, Wells GA, Vandemheen K, et al. The Canadian CT Head Rule for patients with minor head injury. *Lancet* 2001; 357: 1391–1396.
12. Zee CS, Go JL. CT of head trauma. *Neuroimaging Clin N Am* 1998; 8: 525–539.
13. Lee H, Wintermark M, Gean AD, et al. Focal lesions in acute mild traumatic brain injury and neurocognitive outcome: CT versus 3T MRI. *J Neurotrauma* 2008; 25: 1049–1056.
14. Gentry LR, Godersky JC, Thompson B, Dunn VD. Prospective comparative study of intermediate-field MR and CT in the evaluation of closed head trauma. *AJR Am J Roentgenol* 1988; 150: 673–682.
15. Orrison WW, Gentry LR, Stimac GK, et al. Blinded comparison of cranial CT and MR in closed head injury evaluation. *AJNR Am J Neuroradiol* 1994; 15: 351–356.

DOI:10.1002/MSJ

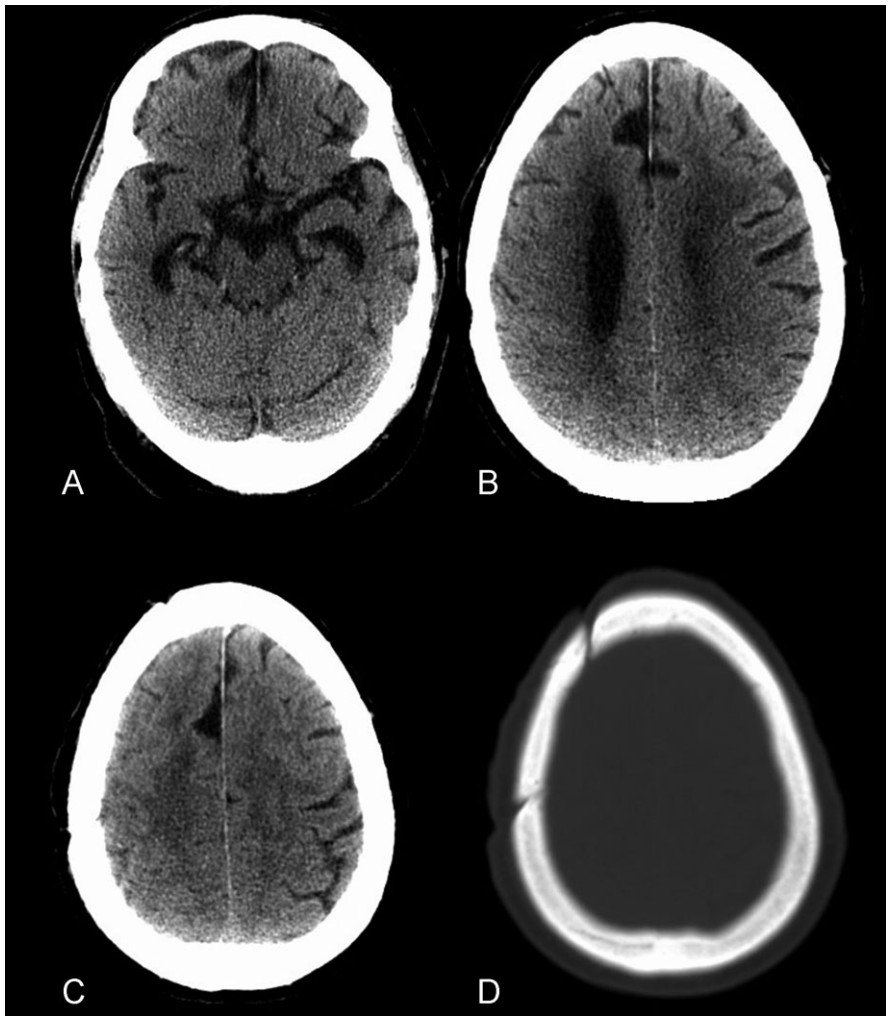

Fig 19. Posttraumatic hydrocephalus. (A,B) The axial computed tomography images show dilatation of the ventricles, including the temporal horns, bilaterally. (C) There is partial effacement of the convexity sulci, which indicates that the enlargement of the ventricles is partially due to hydrocephalus. (D) An image displayed in the bone window shows evidence of a right frontal craniotomy from decompression of a prior intracranial hemorrhage.

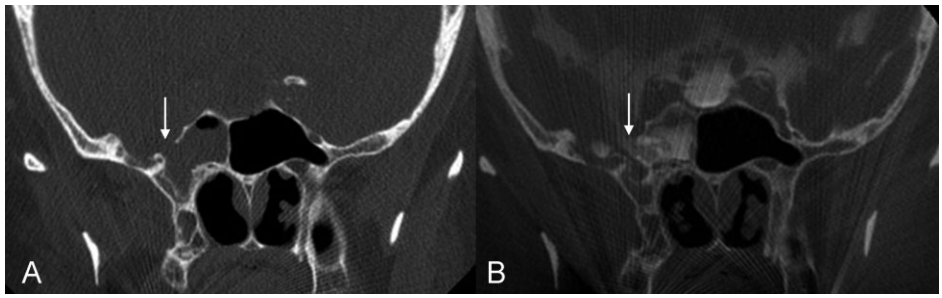

Fig 20. Cerebrospinal fluid leak. (A) The coronal computed tomography image shows a bony defect of the right sphenoid sinus (arrow). (B) The coronal computed tomography image from a cisternogram shows leakage of contrast into the right sphenoid sinus through the bony defect.

DOI:10.1002/MSJ

16. Noguchi K, Ogawa T, Seto H, et al. Subacute and chronic subarachnoid hemorrhage: diagnosis with fluid-attenuated inversion-recovery MR imaging. *Radiology* 1997; 203: 257–262.
17. Woodcock RJ Jr, Short J, Do HM, et al. Imaging of acute subarachnoid hemorrhage with a fluid-attenuated inversion recovery sequence in an animal model: comparison with non-contrast-enhanced CT. *AJNR Am J Neuroradiol* 2001; 22: 1698–1703.
18. Frigon C, Jardine DS, Weinberger E, et al. Fraction of inspired oxygen in relation to cerebrospinal fluid hyperintensity on FLAIR MR imaging of the brain in children and young adults undergoing anesthesia. *AJR Am J Roentgenol* 2002; 179: 791–796.
19. Pruessmann KP, Weiger M, Scheidegger MB, Boesiger P. SENSE: sensitivity encoding for fast MRI. *Magn Reson Med* 1999; 42: 952–962.
20. Sodickson DK, Manning WJ. Simultaneous acquisition of spatial harmonics (SMASH): fast imaging with radiofrequency coil arrays. *Magn Reson Med* 1997; 38: 591–603.
21. Liu AY, Maldjian JA, Bagley LJ, et al. Traumatic brain injury: diffusion-weighted MR imaging findings. *AJNR Am J Neuroradiol* 1999; 20: 1636–1641.
22. Huisman TA, Sorensen AG, Hergan K, et al. Diffusion-weighted imaging for the evaluation of diffuse axonal injury in closed head injury. *J Comput Assist Tomogr* 2003; 27: 5–11.
23. Le TH, Mukherjee P, Henry RG, et al. Diffusion tensor imaging with three-dimensional fiber tractography of traumatic axonal shearing injury: an imaging correlate for the posterior callosal "disconnection" syndrome: case report. *Neurosurgery* 2005; 56: 189.
24. Niogi SN, Mukherjee P, Ghajar J, et al. Extent of microstructural white matter injury in postconcussive syndrome correlates with impaired cognitive reaction time: a 3T diffusion tensor imaging study of mild traumatic brain injury. *AJNR Am J Neuroradiol* 2008; 29: 967–973.
25. Sinson G, Bagley LJ, Cecil KM, et al. Magnetization transfer imaging and proton MR spectroscopy in the evaluation of axonal injury: correlation with clinical outcome after traumatic brain injury. *AJNR Am J Neuroradiol* 2001; 22: 143–151.
26. Lewine JD, Davis JT, Bigler ED, et al. Objective documentation of traumatic brain injury subsequent to mild head trauma: multimodal brain imaging with MEG, SPECT, and MRI. *J Head Trauma Rehabil* 2007; 22: 141–155.
27. Lewine JD, Davis JT, Sloan JH, et al. Neuromagnetic assessment of pathophysiologic brain activity induced by minor head trauma. *AJNR Am J Neuroradiol* 1999; 20: 857–866.
28. Newton MR, Greenwood RJ, Britton KE, et al. A study comparing SPECT with CT and MRI after closed head injury. *J Neurol Neurosurg Psychiatry* 1992; 55: 92–94.
29. Bergsneider M, Hovda DA, McArthur DL, et al. Metabolic recovery following human traumatic brain injury based on FDG-PET: time course and relationship to neurological disability. *J Head Trauma Rehabil* 2001; 16: 135–148.
30. Gross H, Kling A, Henry G, et al. Local cerebral glucose metabolism in patients with long-term behavioral and cognitive deficits following mild traumatic brain injury. *J Neuropsychiatry Clin Neurosci* 1996; 8: 324–334.
31. Alavi A. Functional and anatomic studies of head injury. *J Neuropsychiatry Clin Neurosci* 1989; 1: S45–S50.
32. Al-Nakshabandi NA. The swirl sign. *Radiology* 2001; 218: 433.
33. Greenberg J, Cohen WA, Cooper PR. The "hyperacute" extraaxial intracranial hematoma: computed tomographic findings and clinical significance. *Neurosurgery* 1985; 17: 48–56.
34. Gean AD, Kates RS, Lee S. Neuroimaging in head injury. *New Horiz* 1995; 3: 549–561.
35. Jennett B, Adams JH, Murray LS, Graham DI. Neuropathology in vegetative and severely disabled patients after head injury. *Neurology* 2001; 56: 486–490.
36. Inglese M, Makani S, Johnson G, et al. Diffuse axonal injury in mild traumatic brain injury: a diffusion tensor imaging study. *J Neurosurg* 2005; 103: 298–303.
37. Mittl RL, Grossman RI, Hiehle JF, et al. Prevalence of MR evidence of diffuse axonal injury in patients with mild head injury and normal head CT findings. *AJNR Am J Neuroradiol* 1994; 15: 1583–1589.
38. Scheid R, Preul C, Gruber O, et al. Diffuse axonal injury associated with chronic traumatic brain injury: evidence from T2*-weighted gradient-echo imaging at 3 T. *AJNR Am J Neuroradiol* 2003; 24: 1049–1056.
39. Adams JH, Graham DI, Gennarelli TA, Maxwell WL. Diffuse axonal injury in non-missile head injury. *J Neurol Neurosurg Psychiatry* 1991; 54: 481–483.
40. Ashikaga R, Araki Y, Ishida O. MRI of head injury using FLAIR. *Neuroradiology* 1997; 39: 239–242.
41. Hesselink JR, Dowd CF, Healy ME, et al. MR imaging of brain contusions: a comparative study with CT. *AJR Am J Roentgenol* 1988; 150: 1133–1142.
42. Arfanakis K, Haughton VM, Carew JD, et al. Diffusion tensor MR imaging in diffuse axonal injury. *AJNR Am J Neuroradiol* 2002; 23: 794–802.
43. Gentry LR. Head trauma. In: Atlas SW, ed. *Magnetic Resonance Imaging of the Brain and Spine*. 2nd ed. Philadelphia, PA: Lippincott-Raven; 1996; 611–647.
44. Gean AD. *Imaging of Head Trauma*. Philadelphia, PA: Williams & Wilkins-Lippincott; 1994; 76.
45. Le TH, Gean AD. Imaging of head trauma. *Semin Roentgenol* 2006; 41: 177–189.

DOI:10.1002/MSJ